

## Preparation and application of novel multi-walled carbon nanotubes/polysulfone nanocomposite membrane for chiral separation

Yibing Ji, Jian Ke, Feifei Duan, Jianqiu Chen\*

School of Science, China Pharmaceutical University, Nanjing 210009, China, email: jiyibing@msn.com (Y. Ji), kejiancpu@163.com (J. Ke), 15605197789@163.com (F. Duan), Tel. +86-258-6185150, cjqermembrane@163.com (J. Chen)

Received 5 February 2017; Accepted 10 August 2017

### ABSTRACT

The novel  $\beta$ -cyclodextrin-carboxylated multi walled carbon nanotubes (cMWCNTs)/polysulfone nanocomposite membranes with variable amount of nanoparticle were prepared by wet phase inversion method. Effects of the amount of  $\beta$ -CD-cMWCNTs supramolecular hybrid material on membrane morphology, rejection of bovine serum albumin (BSA), permeation and enantioselectivity were examined. The morphology and chemical compositions of these nanocomposite membranes were characterized by scanning electron microscope (SEM) and attenuated total reflection fourier transform infrared (ATR-FTIR) spectroscopy, respectively. Furthermore, water flux, rejection of BSA and enantioselectivity were used to evaluate the performance of these nanocomposite membranes. As for the enantioseparation of tryptophan enantiomers, filtration experiments were carried out using a dead-end filtration cell holding a flat sheet membrane. In addition, the complete separation of tryptophan racemates can be achieved using a separation system based on multi-stage filtration separation of this novel nanocomposite membrane.

*Keywords:* Enantiomeric separation; Multi-stage filtration; Nanocomposite membranes; Racemic tryptophan

### 1. Introduction

Chirality is a widespread phenomenon that plays a crucial role in nature. The majority of drugs are racemic mixtures which have two enantiomers [1–5]. In general, one of them has the effective therapeutic function while another one may lead to some negative effect or toxicity [6–9]. Therefore, single enantiomer of chiral substances with each enantiomer having different biological activity is in demand [10,11]. A variety of separation methods have been described for the chiral resolution of two enantiomers, including capillary electrophoresis (CE) [12], high performance liquid chromatography (HPLC) [13], crystallization [14], extraction [15], etc. Most of these methods have some disadvantages of high cost of operation, a poor separation effect, high energy consumption and discontinuous operation, which limit the application in industrial production [16–19]. However, membrane-based racemic separation process is a newly emerging, which has several advantages,

such as low energy consumption, simplicity in set-up, and continuous operation mode [16,20–22] and meanwhile promising technology that has been receiving increasing attentions recently.

The chiral resolution in a membrane system can be divided into liquid and solid membranes system. As per the chiral resolution method developed earlier, liquid membrane have good permeability and selectivity to enantiomers, however, its life-time is short due to its poor durability and stability. Compared with liquid membranes, solid membranes provided good stability, favorable permeability and enantioselectivity. Hence, solid films are widely used in industrial production. However, one of the major difficulties in the chiral separation of solid membranes is the low separation factor compared to conventional methods, making it difficult to achieve single-membrane processes [23–27]. A multi-stage cascade in the membrane process has the advantage of using components from existing analytical separation methods, and significantly enhancing the enantiomeric excess, providing an alternative for the current large-scale enantiomer separation processes [28].

\*Corresponding author.

For membrane filtration, polysulfone (PSf)-based membranes are the most widely used because of their excellent heat resistance, chemical stability, good film-forming properties and electrical resistance over a wide pH range. Nevertheless, the foremost drawbacks of the polysulfone membrane materials are the essentially hydrophobic, whereas the filtration membranes require considerable hydrophilicity in order to cope with the problem of productivity. In addition, the general membranes suffer from fouling, thus resulting in low membrane life time. The low permeability and fouling are mainly owing to low surface hydrophilicity and low porosity. Therefore, researchers are looking for a membrane with finely-balanced characteristics [4,29].

Since the 1990s, carbon nanotubes (CNTs) have attracted a great deal of attention of researches in the fields of chemistry, physics and materials science [30]. However, in order to improve their dispersibility in typical organic solvents owing to their chemically inert properties, many efforts of investigators have been focused on the functionalization and modification of CNTs [31,32]. Functionalized CNTs can offer the opportunity to alter various membrane properties, including surface chemistry, pore size, tensile strength, and solute rejection by incorporating them into casting solution due to their excellent physical, mechanical, electrical and optical properties. Even in quantities as low as 0.1% by weight of the final polymer membrane [33–36].

In the present work, in order to improve the enantioselectivity and water flux of the polysulfone membrane carboxylated MWCNTs were functionalized with  $\beta$ -cyclodextrin ( $\beta$ -CD) [37]. The functionalized cMWCNTs were then incorporated into polysulfone polymer matrix to form the nanocomposite membranes. In addition, the current study investigated the effect of adding various concentrations of functionalized cMWCNTs on the morphology, performance and enantioselectivity of polysulfone nanocomposite membranes. Membrane performance was characterized by water flux and bovine serum albumin (BSA) rejection. The nanocomposite membranes were used for the separation of racemic tryptophan, which of concentration is 0.025 g/L.

## 2. Experimental

### 2.1. Materials

Carboxylated multi-walled carbon nanotubes with an outer diameter of 10–20 nm, and length 0.5–2  $\mu$ m (purity  $\geq$ 95 wt.) were purchased from Nanjing XFNANO Materials Tech Co., Ltd., China. Polysulfone polymer (molecular weight: 77–83 kg/mol) was provided by Shanghai Shuao Chemical Co., Ltd., China.  $\beta$ -cyclodextrin ( $\beta$ -CD), DL-tryptophan L-tryptophan,  $\gamma$ -(2,3-epoxypropoxy) propyltrimethoxysilane (GPTMS), polyethylene glycol (PEG400) were purchased from Aladdin Co. (Shanghai, China). N,N-dimethylformamide (DMF), N,N-dimethylacetamide (DMAc), acetone were obtained from Nanjing Chemical Reagent Company, China. Bovine serum albumin (BSA) was obtained from Sigma-Aldrich (Shanghai, China). All reagents used in the experiments were of analytical grade. Deionized water was used throughout all experiments.

### 2.2. Preparation of $\beta$ -CD/cMWCNTs supramolecular hybrid material

$\beta$ -CD/cMWCNTs were synthesized using a He's method [37]. 5 g of pre-dried  $\beta$ -CD was weighed into a round-bottomed flask containing 40 mL of DMF. 5.9 mL of the GPTMS solution was slowly added to the flask, whereupon the dissolved  $\beta$ -CD was precipitated and stirred to ensure then completely dissolved, and then 0.1 g of sodium hydroxide was placed into the solution to maintain the entire solution in an alkaline environment. The flask was stirred in an oil bath at 55°C for 48 h within nitrogen atmosphere. The reaction solution was transferred to a beaker and cooled to room temperature after completion of the reaction. Meanwhile, the product was precipitated and filtered using a large amount of acetone completely. The final filtered product was dried overnight in a vacuum oven at 40°C to give a light yellow solid powder.

2 g of the above-mentioned light yellow solid powder was dissolved in 30 ml of distilled water under constant stirring, and the pH of the solution was adjusted to between 4 and 6 by acetic acid, and the product of hydrolysis was obtained after stirring for 1 h. Afterwards, 0.2 g cMWCNTs were accurately weighed into the above reaction solution, and ultrasonicated for 40 min to disperse the CNTs in the solution homogeneously. Refluxing at 90°C for 10 h. The resulting solution was washed repeatedly to remove the residue and then filtered with a large amount of deionized water. It was dried in a vacuum oven at 80°C overnight. This synthesis is presented in Fig. 1.

### 2.3. Preparation of the chiral nanocomposite membrane

$\beta$ -CD-cMWCNTs/polysulfone nanocomposite membranes were fabricated by the phase inversion method [38,39]. The compositions of the casting solutions are shown in Table 1. The polysulfone polymer was dried in a vacuum oven at 120°C for 24 h before using. Polymer nanocomposite solutions for membrane formation were prepared in N, N-dimethylacetamide (DMAc) with 15 wt.% PSF and 8 wt.% polyethylene glycol (PEG400) with respect to the total volume of solution. Different  $\beta$ -CD-cMWCNTs/polysulfone nanocomposite membranes were obtained using mixtures of 0, 0.1, 0.5, and 1 wt.%  $\beta$ -CD-cMWCNTs. The above-mentioned polymer nanocomposite solutions was under continuous stirring at 50°C for 3 h. Afterwards, the  $\beta$ -CD-cMWCNTs was dispersed throughout the homogeneous polymer solution, first by sonication for 30 min, followed by vigorously stirring for 3 h at 50°C. The fully dissolved casting solution was rested overnight for degassing. The casting solution was spread on a clean glass using a doctor blade to form a homogeneous film. After 30 s of exposure in air, the nascent membrane was immersed into deionized water bath and phase inversion occurred through solvent/non-solvent stratification. The formed membrane was floated from the glass surface and rinsed with deionized water to remove the residual solvent. Membranes were kept in deionized water for at least 24 h before using. Process temperature (25°C  $\pm$  2°C) and humidity (62%  $\pm$  2%) were monitored and determined to be constant.

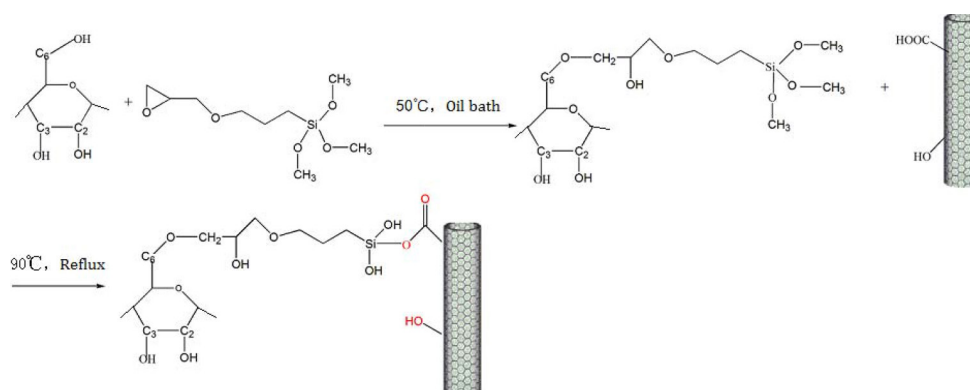


Fig. 1. The chemical reactions of the GPTMS-β-CD-cMWCNTs synthesis.

Table 1  
Composition of casting solution and characteristics of nanocomposite membrane

Polysulfone (wt.%)	PEG (400)	β-CD-cMWCNTs (wt.%)	Thickness (mm)	Porosity (%)	Pore radius (nm)
15	8	0	0.125	82	3.20
15	8	0.1	0.198	84	12.5
15	8	0.5	0.129	86	16.3
15	8	1	0.126	87	20.2

#### 2.4. Characterization of the β-CD-cMWCNTs/PSF nanocomposite membrane

The chemical structure of functional groups on the membrane surface was characterized by attenuated total reflection Fourier transform infrared spectroscopy (ATR-FTIR) (Nexus 870 FT-IR Nicolet, USA). The membrane samples were rinsed with pure water and dried in a drier to remove moisture from the membrane surface before use.

The morphology of the surface and cross-section of the films was investigated by scanning electron microscopy (SEM) (3400N scanning electron microscope, Hitachi, Tokyo, Japan). Cross-sectional membrane samples were freeze-dried and quenched in liquid nitrogen to ensure the structural integrity of the sections. Finally, sputter-coated with gold.

The porosity ( $\varepsilon$ ) of all the membranes was calculated according to a gravimetric method defined in Eq. (1) [40,41]

$$\varepsilon = \frac{W_{wet} - W_{dry}}{A * L * \rho_w} \quad (1)$$

where  $W_{wet}$  is the mass of membrane immersed in pure water for 72 h,  $W_{dry}$  is the mass of the membrane after dried for 24 h in a vacuum oven at 80°C,  $A$  is the effective membrane area ( $m^2$ ),  $L$  is the thickness of the membrane (m). The density of water  $\rho_w$  is 0.997 g/cm<sup>3</sup>.

The average pore diameter of the nanocomposite film,  $r_m$ , was measured by the following Guerout–Elford–Ferry equation as shown in Eq. (2) [42,43]

$$r_m = \sqrt{\frac{(2.90 - 1.75\varepsilon)8\eta LQ}{\varepsilon A \Delta P}} \quad (2)$$

where  $\varepsilon$  is the porosity of the membrane, the viscosity of the water ( $\eta$ ) is  $8.9 \times 10^{-4}$  Pa s,  $L$  is the thickness of the membrane (m),  $Q$  is the pure water permeation rate ( $m^3/s$ ),  $A$  is the effective membrane Area ( $m^2$ ), and the pressure at the time of measurement ( $\Delta P$ ) is 0.1 MPa.

The pure water flux and protein rejection of the membranes were obtained by ultrafiltration test system at an operation pressure of 0.1 MPa. Each membrane, which of the active area is 19.6 cm<sup>2</sup>, was supported in the cell by a porous stainless steel disk.

The water flux was calculated in Eq. (3)

$$J = \frac{V}{At} \quad (3)$$

where  $J$  is the permeation flux of membrane ( $L/(m^2h)$ ),  $V$  is the total volume of permeated pure water (L),  $A$  is the active area of membrane ( $m^2$ ), and  $t$  is the operation time (h).

The protein rejection was measured with 1.0 g/L BSA solution at an operation pressure of 0.1 MPa. The concentrations of the permeation and feed solutions were determined by an ultraviolet–visible spectrophotometer (Lambda 35, PerkinElmer, USA) at 280 nm. The rejection was calculated in Eq. (4)

$$R(\%) = 100 \left( 1 - \frac{C_p}{C_f} \right) \quad (4)$$

where  $R$  is the BSA rejection, and  $C_f$ ,  $C_p$  represent BSA concentrations in the feed and permeate solution, respectively.

#### 2.5. Separation of tryptophan enantiomer

Filtration experiments were performed using a dead-end filter cell maintaining a flat sheet membrane. The flow

diagram of a multi-stage filtration process is shown in Fig. 2. Aqueous solution of racemic tryptophan was forced to repeatedly permeate through the  $\beta$ -CD-cMWCNTs/PSF nanocomposite membranes at a constant flow rate of 0.1 ml/min in the membrane microdevice.

The collected filtrate was analyzed using a chiral ligand exchange chromatography method [44] on a 1200 infinity series HPLC (Agilent Technologies, America). The concentration of permeate solution was performed at 35°C using a mobile phase containing 0.375 mM L-phenylalanine and 0.075 mM copper sulfate as chiral ligand exchange reagent as well as methanol/water (20:80, v/v) at a flow rate of 1.0 mL/min. Detection wavelength of tryptophan was 278 nm. Enantioselectivity was replaced in terms of percent enantiomeric excess (e.e.%). The equations were as follows:

$$e.e.(%) = 100 \frac{A_D - A_L}{A_D + A_L} \quad (5)$$

where  $A_D$  and  $A_L$  denote *D*- and *L*-tryptophan peak area in the chromatogram of the filtrate, respectively.

### 3. Results and discussion

#### 3.1. Characterization of the $\beta$ -CD-cMWCNTs/PSF nanocomposite membrane

##### 3.1.1. IR studies

The FT-IR spectrum of GPTMS- $\beta$ -CD (Fig. 3) shows the stretching vibrations peaks of the  $-\text{CH}_3$ ,  $-\text{CH}_2$  groups, which belong to the functional groups of the silane coupling agent (GPTMS), at 2930 and 2887  $\text{cm}^{-1}$ , respectively. The S-O-Si absorption band and the stretching vibrations of the Si-O-Si group were associated with peaks at around 758  $\text{cm}^{-1}$  and 1038  $\text{cm}^{-1}$ , respectively. The peak at 1161  $\text{cm}^{-1}$  was because of the C-O-C group of glucose units. Other peaks at 3393 and 1665  $\text{cm}^{-1}$  were attributable to the bending vibration and stretching vibration of the  $-\text{OH}$  group, respectively. All the peaks indicated that GPTMS- $\beta$ -CD has been successfully synthesized.

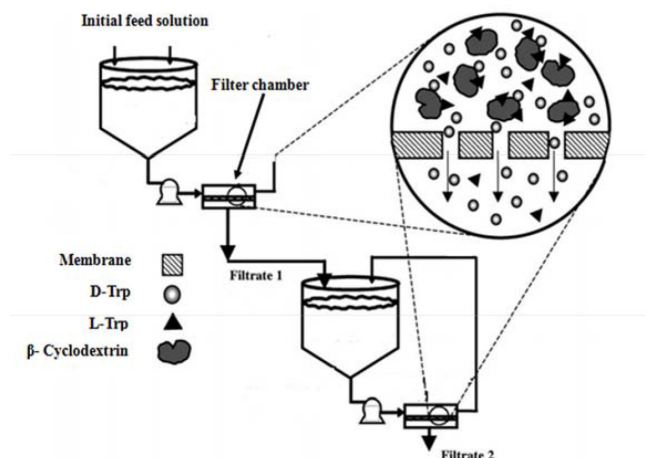


Fig. 2. The flow diagram of a multi-stage filtration process.

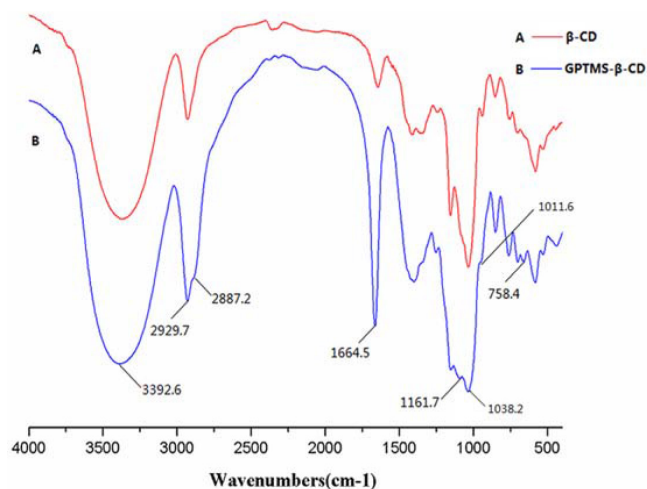


Fig. 3. FT-IR spectra of GPTMS- $\beta$ -CD and  $\beta$ -CD.

The FT-IR spectra of cMWCNTs and GPTMS- $\beta$ -CD-cMWCNTs are shown in Fig. 4. The absorption peaks between 3100–3533  $\text{cm}^{-1}$  belong to  $-\text{OH}$  characteristic peaks. The stretching vibration peaks of  $-\text{C}=\text{O}$  were associated with peaks at 1636, 1583  $\text{cm}^{-1}$ . The peaks at 2927 and 1014  $\text{cm}^{-1}$  were the result of the stretching vibration peaks of  $-\text{CH}_2$  and  $-\text{COC}$  on the cyclodextrin. The peaks at 1633 and 1581  $\text{cm}^{-1}$  were because of the absorption peak of  $-\text{COOH}$  on multi-walled carbon nanotube. The peaks at 756 and 1084  $\text{cm}^{-1}$  were attributable to the absorption peak of Si-O-Si groups. It was confirmed that GPTMS- $\beta$ -CD was successfully modified to carboxylated MWCNTs.

Once the nanocomposite membranes were dried by air completely, the ATR-FTIR spectra were recorded. Fig. 5 shows the ATR-FTIR spectra of  $\beta$ -CD-cMWCNTs/PSF nanocomposite membrane. ATR-FTIR spectra displaying peaks at around 1106, 1150, 1242, 1294, 1323, 1488, 1585  $\text{cm}^{-1}$  are the characteristics of the polysulfone membrane material. The Si-O-Si weak absorption band were associated with the peak at 756  $\text{cm}^{-1}$  and the peak at 1037  $\text{cm}^{-1}$  was attributable to the stretching vibrations of the Si-O-Si group. Also peaks between 2931  $\text{cm}^{-1}$  and 1014  $\text{cm}^{-1}$  correspond to the stretching vibrations of  $-\text{CH}_2-$  and  $-\text{C}-\text{O}-\text{C}-$  groups of  $\beta$ -CD, respectively.

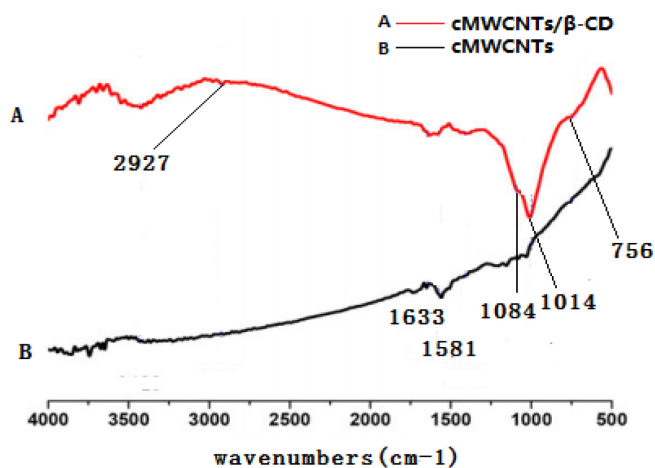


Fig. 4. FT-FTIR spectra of  $\beta$ -CD-cMWCNTs and cMWCNTs.

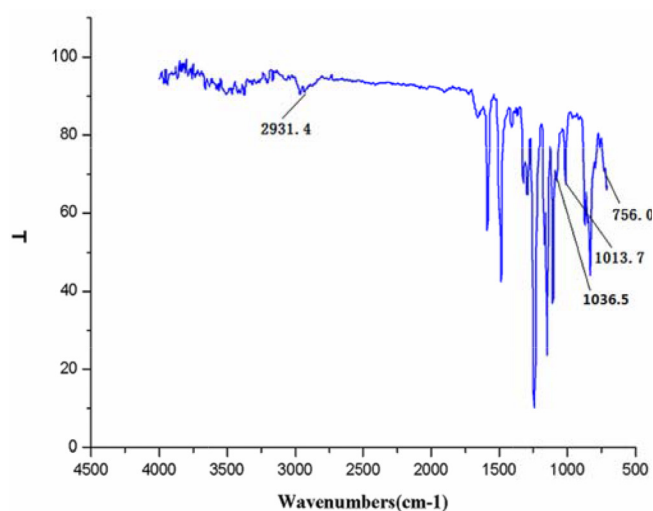


Fig. 5. ATR-FTIR spectra of  $\beta$ -CD-cMWCNTs/PSF nanocomposite membrane.

### 3.1.2. Morphologies of the $\beta$ -CD-cMWCNTs/PSF nanocomposite membranes

The pore structure of the nanocomposite film is considered to be a function of a series of variables, including: viscosity of casting solution, the polymer chain packing or free volume after deposition, and the agglomeration state of the nanoparticles [45–47]. The presence of  $\beta$ -CD-cMWCNTs will affect the pore structure of the membrane by influencing these variables.

Fig. 6 shows the surface and cross sectional SEM images of PSF and  $\beta$ -CD-cMWCNTs/PSF nanocomposite

membranes. It was observed that  $\beta$ -CD-cMWCNTs incorporation produces significant changes in both upper and support layer morphology. Visually, surface porous and cross section macro-voids were altered. From SEM images it can be observed that with the incorporation of  $\beta$ -CD-cMWCNTs, the porous and macro-voids dimension increased. The pores and macro-voids dimensions are approximately twice over for the composite and more interconnected or finger-like pore structure in the sub layer is visible in the nanocomposite membrane with highest  $\beta$ -CD-cMWCNTs loading. This phenomenon can be explained taking into account the structure of the  $\beta$ -CD-cMWCNTs. The  $\beta$ -CD-cMWCNTs plays a significant role in the solvent/non-solvent exchange during phase inversion process by blocking the molecules passage through the composite material bulk. Therefore the exchange of solvents is realized on the available pathways and results in the formation of extended size pores and macro-voids.

### 3.2. Performance evaluation of membranes

#### 3.2.1. Effect of $\beta$ -CD-cMWCNTs loading on the membrane properties

The nanocomposite membranes containing  $\beta$ -CD-cMWCNTs content from 0 to 1 wt% were prepared to investigate the influence of  $\beta$ -CD-cMWCNTs loading on the membrane performance. Fig. 7 shows the effect of  $\beta$ -CD-cMWCNTs content in the casting solution on rejection and the pure water flux of resulting  $\beta$ -CD-cMWCNTs/PSF nanocomposite membranes. When the  $\beta$ -CD-cMWCNTs content was 1% (wt.), the maximum pure water flux were obtained. Beyond that, the casting solution is difficult to form a stable and homogeneous solution.

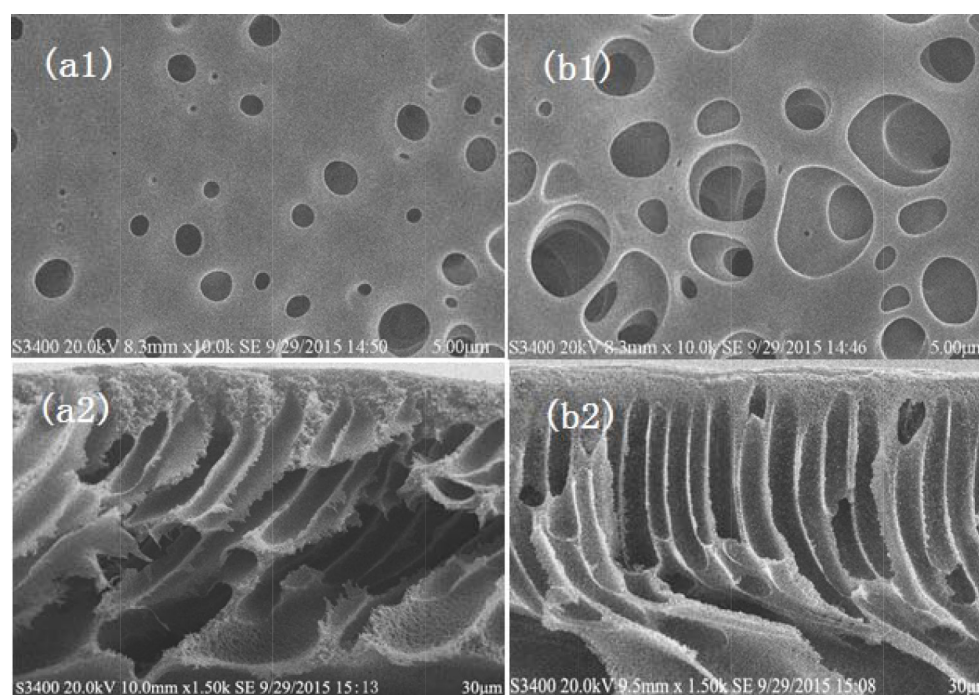


Fig. 6. SEM micrographs of (a1), (b1) surface of the PSF and  $\beta$ -CD-cMWCNTs/PSF membranes (1 wt%), respectively, (a2), (b2) cross-section of the PSF and  $\beta$ -CD-cMWCNTs/PSF membranes (1 wt%), respectively.

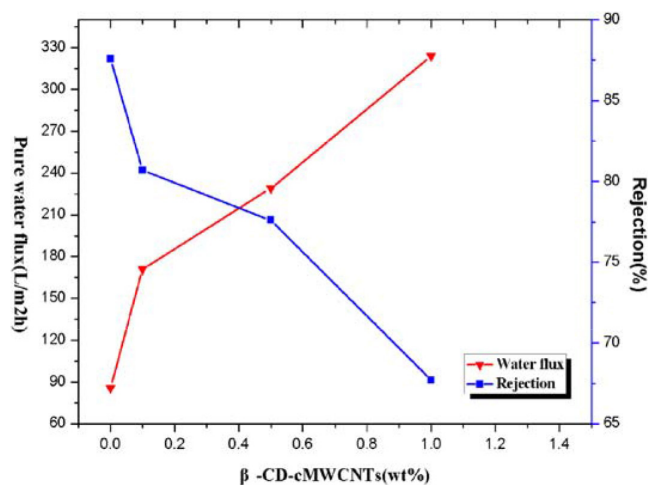


Fig. 7. Effect of  $\beta$ -CD-cMWCNTs content on the pure water flux and rejection to BSA albumin of  $\beta$ -CD-cMWCNTs/PSF nanocomposite membrane at 0.1 MPa operation pressure.

The enhancement of flux is due to two reasons. First, the more content of  $\beta$ -CD-cMWCNT, the higher hydrophilicity, which could induce an increase in pure water flux, of the nanocomposite film. Second, from data in Table 1, it was observed that the pore radius of the membranes increased with  $\beta$ -CD-cMWCNTs content up to 1% (wt.). The order of the pore size with the contents of  $\beta$ -CD-cMWCNTs was: 0% < 0.1% < 0.5% < 1%. The order of increasing pore size is consistent with the increasing order of water flux. It can be concluded that the increase of water flux is affected by the pore size of the membrane. However, the rejection rate of BSA was the reverse of the increase of water flux, and the rejection rate of BSA decreased with the increase of GPTMS- $\beta$ -CD-cMWCNTs content. This is mainly due to the increased pore size of the membrane surface leading to a gradual decrease in BSA rejection depicted in Fig. 7 and Table 1.

The data for some quantitative properties of the membrane are tabulated in Table 1. The total porosity and the mean pore radius of the nanocomposite films increase with the addition of  $\beta$ -CD-cMWCNTs from 0 to 1 wt.%. The maximum porosity and pore diameter can be obtained when the nanoparticle content is 1%. The steric hindrance and electrostatic interaction between  $\beta$ -CD-cMWCNTs and PSF may play an important role in the increase of membrane pore size [25].

### 3.2.2. Effect of pH of buffer solution on the tryptophan enantiomers separation

The impact of pH value of PBS solution on the separation of tryptophan enantiomers was investigated. From Fig. 8 it can be seen that at the isoelectric point of tryptophan (pH 5.90), a largest enantiomeric excess that is the average of three replicates was obtained. The enantiomeric excess decreased whether pH of the buffer solution is less than or greater than the isoelectric point of the tryptophan.

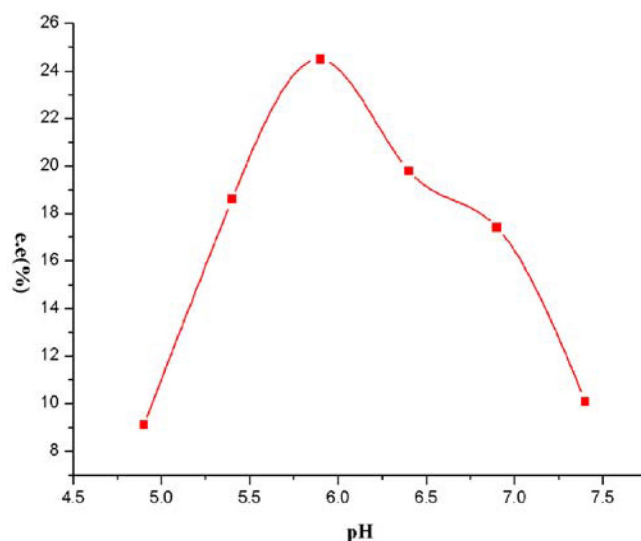


Fig. 8. Influence of pH of buffer solution on the tryptophan enantiomers separation.

When the pH of the solution is approaching to 5.9, which is the isoelectric point of tryptophan, the tryptophan is neutral, at which time it can be better combined with cyclodextrin, whose hydrophilic groups were exposed from the hydrophobic cavity.

### 3.2.3. Effect of $\beta$ -CD-cMWCNTs loading on the separation of tryptophan enantiomers

Table 2 and Fig. 9 show the effect of  $\beta$ -CD-cMWCNTs content in the casting solution on separation efficiency of resulting  $\beta$ -CD-cMWCNTs/PSF nanocomposite membranes. The concentration of D-Trp and L-Trp transported through  $\beta$ -CD-cMWCNTs/PSF nanocomposite membrane was determined using chiral ligand exchange chromatography method.

Two cases were considered. At first, the transportation of D-Trp and L-Trp at the same concentration through PSF membrane showed that the peak area of D-Trp and L-Trp was almost similar, indicating that tryptophan enantiomers could not be separated by PSF membrane because PSF membrane does not have chiral recognition layer. When the PSF membrane was incorporated with  $\beta$ -CD-cMWCNTs,

Table 2  
Effect of  $\beta$ -CD-cMWCNTs loading on the separation of tryptophan enantiomers

$\beta$ -CD-cMWCNTs (wt%)	Peak area		e.e (%) <sup>c</sup>
	AD <sup>a</sup>	AL <sup>b</sup>	
0	334	315	2.93
0.1	334	298	5.66
0.5	336	280	9.13
1	336	204	24.5

<sup>a</sup>D – tryptophan peak area, <sup>b</sup>L – tryptophan peak area, <sup>c</sup>Enantiomeric excess (%).

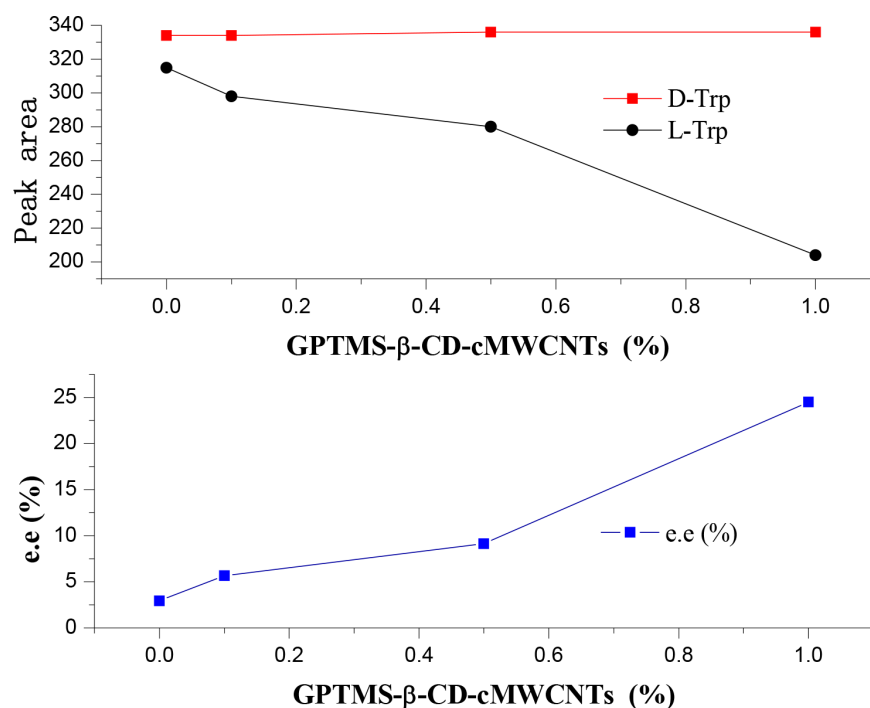


Fig. 9. Effect of  $\beta$ -CD-cMWCNTs loading on the separation of tryptophan enantiomers.

the determination of D-Trp and L-Trp in the filtrate showed that D-tryptophan peak area remains constant while L-tryptophan peak area gradually decreases. With the increase of  $\beta$ -CD-cMWCNTs content, enantiomeric excess values increased significantly. When the  $\beta$ -CD-cMWCNTs content was increased to 1 wt.%, the enantiomeric excess reached a maximum.

### 3.3. Complete separation of tryptophan enantiomers

Fig. 10 shows the chromatogram of each collected filtrate at 25°C. It can be seen that the concentration of L-tryptophan decreased gradually while the concentration of D-tryptophan basically unchanged with the increasing number of the filtration. D, L-tryptophan achieved a

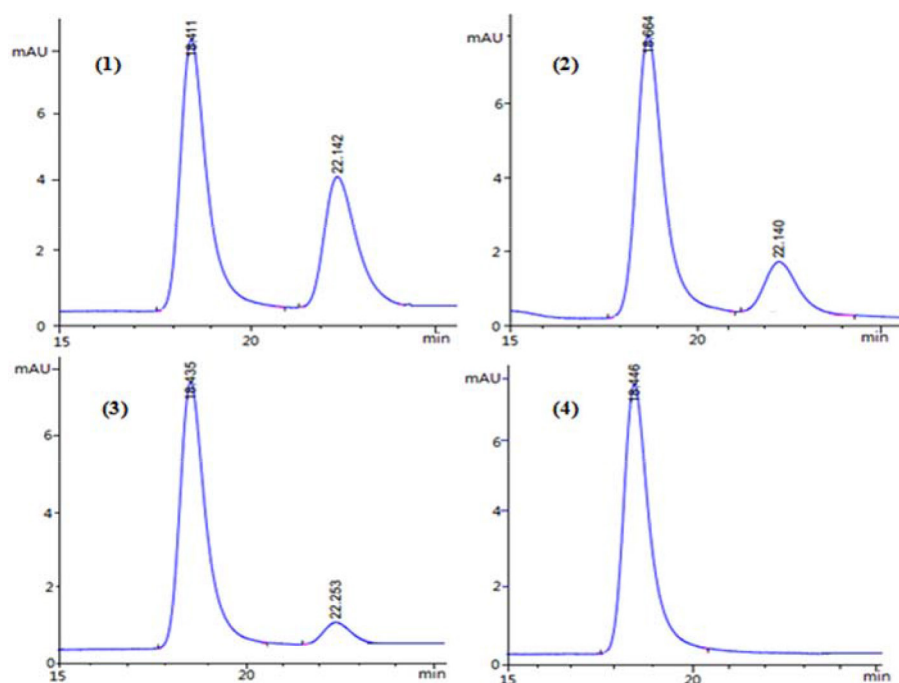


Fig. 10. The chromatogram of each collected filtrate.

completely separated by using this novel nanocomposite membrane based separation system after 4 times filtration.

The chiral separation process by membrane can be achieved only when membrane selectively adsorbs or selectively migrates one of enantiomers. The GPTMS- $\beta$ -CD-cMWCNTs/PSF nanocomposite films prepared play a 'fence' role in the separation of tryptophan enantiomers and selectively retains L-Trp enantiomer owing to stereo-specific sorption between L-Trp and modified  $\beta$ -CD resided inside the membrane. The enantiomer which has strong interaction with chiral recognition sites may transport slowly through the membrane and the counter enantiomer diffuses rapidly.

#### 4. Conclusions

The carboxylated multi-walled carbon nanotubes were functionalized with modified  $\beta$ -CD. Polysulfone and  $\beta$ -CD-cMWCNTs/polysulfone nanocomposite membranes with different weight concentration of  $\beta$ -CD-cMWCNTs (0, 0.1, 0.5, and 1 wt.%) were fabricated by phase inversion method. From SEM images, it can be seen that the morphology of the membranes was changed with the incorporation of  $\beta$ -CD-cMWCNTs, the pores and macro-voids dimensions are increased and more interconnected or finger-like pore structure in the support layer. The incorporation of  $\beta$ -CD-cMWCNTs into casting solution significantly improved water flux. This is believed to have resulted, either from the creation of connection channels between membrane pores, or an increase in the hydrophilic nature of the membrane due to the functionalized MWCNTs. Bovine serum albumin rejection was found to decrease for the incorporation of  $\beta$ -CD-cMWCNTs because of the larger surface pore size.

Experimental results shows that  $\beta$ -CD-cMWCNTs/PSF nanocomposite membrane can selectively adsorbs L-enantiomer of DL-tryptophan, and a complete separation of tryptophan can be achieved with a multi-stage filtration system. Through our results, it can be found that the novel nanocomposite membrane-based separation system can greatly increase the resolution of enantiomers. As this method is suitable for wide range of chiral selectors, including cyclodextrin and its derivatives, and the system is relatively simple and straight forward using available modules, it has great application prospects for many chiral substances separation.

#### Acknowledgments

The authors greatly appreciate the financial supports of the fundamental research funds for central universities (No. JKZ2011009) and "333" Project of Jiangsu Province.

#### References

- [1] Y. Sueyoshi, C. Fukushima, M. Yoshikawa, Molecularly imprinted nanofiber membranes from cellulose acetate aimed for chiral separation, *J. Membr. Sci.*, 357 (2010) 90–97.
- [2] S. Bozkurt, M. Yilmaz, A. Sirit, Chiral calix[4]arenes bearing amino alcohol functionality as membrane carriers for transport of chiral amino acid methyl esters and mandelic acid, *Chirality*, 24 (2012) 129–136.
- [3] J.J. Ha, H.J. Choi, J.S. Jin, E.D. Jeong, M.H. Hyun, Liquid chromatographic resolution of proton pump inhibitors including omeprazole on a ligand exchange chiral stationary phase, *J. Chromatogr. A*, 1217 (2010) 6436–6441.
- [4] K. Singh, P.G. Ingole, H.C. Bajaj, H. Gupta, Preparation, characterization and application of  $\beta$ -cyclodextrin-glutaraldehyde crosslinked membrane for the enantiomeric separation of amino acids, *Desalination*, 298 (2012) 13–21.
- [5] X.W. Yu, Y. Xu, H. Gu, Enhancement of chiral resolution of dl-menthol at high substrate concentration by in situ resin adsorption, *J. Biotechnol.*, 150 (2010) S345–S345.
- [6] W.F. Wang, W.W. Xiong, M. Zhao, W.Z. Sun, F.R. Li, L.M. Yuan, Chiral separation of trans-stilbene oxide through cellulose acetate butyrate membrane, *Tetrahedron-Asymmetr.*, 20 (2009) 1052–1056.
- [7] Y.J. Wang, Y. Hu, H. Xu, G.S. Luo, Y.Y. Dai, Immobilization of lipase with a special microstructure in composite hydrophilic CA/hydrophobic PTFE membrane for the chiral separation of racemic ibuprofen, *J. Membr. Sci.*, 293 (2007) 133–141.
- [8] D.Y. Zhang, T.Z. Zhang, J.P. Deng, W.T. Yang, Effect of copolymer composition in poly(N-propargylamide) on helical structure and optical activity, *React. Funct. Polym.*, 70 (2010) 376–381.
- [9] P.G. Ingole, H.C. Bajaj, K. Singh, Membrane separation processes: Optical resolution of lysine and asparagine amino acids, *Desalination*, 343 (2014) 75–81.
- [10] A. Higuchi, M. Tamai, Y.A. Ko, Y.I. Tagawa, Y.H. Wu, B.D. Freeman, J.T. Bing, Y. Chang, Q.D. Ling, Polymeric membranes for chiral separation of pharmaceuticals and chemicals, *Polym. Rev.*, 50 (2010) 113–143.
- [11] Z.H. Zhang, M.L. Zhang, Y.A. Liu, X. Yang, L.J. Luo, S.Z. Yao, Preparation of l-phenylalanine imprinted polymer based on monodisperse hybrid silica microsphere and its application on chiral separation of phenylalanine racemates as HPLC stationary phase, *Sep. Purif. Technol.*, 87 (2012) 142–148.
- [12] M. Riesova, R. Geryk, K. Kalikova, T. Slechtova, M. Voborna, M. Martinkova, A. Bydzovska, E. Tesarova, Direct CE and HPLC methods for enantioseparation of tryptophan and its unnatural derivatives, *Sep. Purif. Technol.*, 158 (2016) 24–30.
- [13] E. Gavioli, N.M. Maier, C. Minguillón, W. Lindner, Preparative enantiomer separation of dichlorprop with a cinchona-derived chiral selector employing centrifugal partition chromatography and high-performance liquid chromatography: a comparative study, *Anal. Chem.*, 76 (2004) 5837–5848.
- [14] D.M. Gotrane, R.D. Deshmukh, P.V. Ranade, S.P. Sonawane, B.M. Bhawal, M.M. Gharpure, M.K. Gurjar, A novel method for resolution of amlodipine, *Org. Process Res. Dev.*, 14 (2010) 640–643.
- [15] T.B. Reeve, J.P. Cros, C. Gennari, U. Piarulli, J.G. de Vries, A practical approach to the resolution of racemic N-benzyl  $\alpha$ -amino acids by liquid-liquid extraction with a lipophilic chiral salen-cobalt(III) complex, *Angew. Chem. Int. Ed.*, 45 (2006) 2449–2453.
- [16] C.O. Ma, X.L. Xu, P. Ai, S.M. Xie, Y.C. Lv, H.Q. Shan, L.M. Yuan, Chiral separation of D,L-mandelic acid, through cellulose membranes, *Chirality*, 23 (2011) 379–382.
- [17] C. Meng, Y. Sheng, Q. Chen, H. Tan, H. Liu, Exceptional chiral separation of amino acid modified graphene oxide membranes with high-flux, *J. Membr. Sci.*, 526 (2017) 25–31.
- [18] Z. Zhou, L. He, Y. Mao, W. Chai, Z. Ren, Green preparation and selective permeation of d-tryptophan imprinted composite membrane for racemic tryptophan, *Chem. Eng. J.*, 310 (2017) 63–71.
- [19] X. Feng, Q. Zhang, X. Liang, J. Li, Y. Zhao, L. Chen, Preparation, characterization and application of a chiral thermo-sensitive membrane for phenylalanine separation of the racemic mixture, *J. Polym. Res.*, 21 (2014) 1–9.
- [20] T. Gumi, A. Valiente, C. Palet, Elucidation of SR-propranolol transport rate and enantioselectivity through chiral activated membranes, *J. Membr. Sci.*, 256 (2005) 150–157.
- [21] P.G. Ingole, H.C. Bajaj, K. Singh, Optical resolution of racemic lysine monohydrochloride by novel enantioselective thin film composite membrane, *Desalination*, 305 (2012) 54–63.

- [22] H.D. Wang, L.Y. Chu, H. Song, J.P. Yang, R. Xie, M. Yang, Preparation and enantiomer separation characteristics of chitosan/ $\beta$ -cyclodextrin composite membranes, *J. Membr. Sci.*, 297 (2007) 262–270.
- [23] K. Shiomi, M. Yoshikawa, Multi-stage chiral separation with electrospun chitin nanofiber membranes, *Sep. Purif. Technol.*, 118 (2013) 300–304.
- [24] S. Robl, L. Gou, A. Gere, M. Sordo, H. Lorenz, A. Mayer, C. Pauls, K. Leonhard, A. Bardow, A. Seidel Morgenstern, K. Schaber, Chiral separation by combining pertraction and preferential crystallization, *Chem. Eng. Process*, 67 (2013) 80–88.
- [25] Y. Matsuoka, N. Kanda, Y.M. Lee, A. Higuchi, Chiral separation of phenylalanine in ultrafiltration through DNA-immobilized chitosan membranes, *J. Membr. Sci.*, 280 (2006) 116–123.
- [26] J. Meng, G. Wei, X.B. Huang, Y. Dong, Y.X. Cheng, C.J. Zhu, A fluorescence sensor based on chiral polymer for highly enantioselective recognition of phenylalaninol, *Polymer*, 52 (2011) 363–367.
- [27] R. Xie, L.Y. Chu, J.G. Deng, Membranes and membrane processes for chiral resolution, *Chem. Soc. Rev.*, 37 (2008) 1243–63.
- [28] J. Romero, A.L. Zydney, Staging of affinity ultrafiltration processes for chiral separations, *J. Membr. Sci.*, 209 (2002) 107–119.
- [29] M. Ionita, A.M. Pandele, L. Crica, L. Pilan, Improving the thermal and mechanical properties of polysulfone by incorporation of graphene oxide, *Compos. Part B Eng.*, 59 (2014) 133–139.
- [30] S. Iijima, Helical microtubules of graphic carbon, *Nature*, 354 (1991) 56–58.
- [31] S. Qiu, L.G. Wu, X.J. Pan, L. Zhang, H.L. Chen, C.J. Gao, Preparation and properties of functionalized carbon nanotube/PSF blend ultrafiltration membranes, *J. Membr. Sci.*, 342 (2009) 165–172.
- [32] S.M. Sanip, A.F. Ismail, P.S. Goh, B.C. Ng, M.S. Abdullah, T. Soga, M. Tanemura, H. Yasuhiko, Preparation and characteristics of functionalized multiwalled carbon nanotubes in polyimide mixed matrix membrane, *ACS Nano*, 5 (2011) 195–202.
- [33] J.H. Choi, J. Jegal, W.N. Kim, Fabrication and characterization of multi-walled carbon nanotubes/polymer blend membranes, *J. Membr. Sci.*, 284 (2006) 406–415.
- [34] E. Celik, H. Park, H. Choi, Carbon nanotube blended polyethersulfone membranes for fouling control in water treatment, *Water Res.*, 45 (2011) 274–282.
- [35] Y. Hou, J. Tang, H.B. Zhang, C. Qian, Y.Y. Feng, J. Liu, Functionalized few-walled carbon nanotubes for mechanical reinforcement of polymeric composites, *ACS Nano*, 3 (2009) 1057–1062.
- [36] H.A. Shawky, S.R. Chae, S.H. Lin, M.R. Wiesner, Synthesis and characterization of a carbon nanotube/polymer nanocomposite membrane for water treatment, *Desalination*, 272 (2011) 46–50.
- [37] Y. He, Z.H. Xu, F. Wu, Q.B. Yang, J. Zhang, Preparation and adsorption studies of  $\beta$ -cyclodextrin grafted onto multi-walled carbon nanotube, *J. Chem. Technol. Biot.*, 90 (2015) 2257–2264.
- [38] J.F. Blanco, J. Sublet, Q.T. Nguyen, P. Schaetzel, Formation and morphology studies of different polysulfones-based membranes made by wet phase inversion process, *J. Membr. Sci.*, 283 (2006) 27–37.
- [39] T.H. Young, L.W. Chen, Pore formation mechanism of membranes from phase inversion process, *Desalination*, 103 (1995) 233–247.
- [40] L.Y. Yu, Z.L. Xu, H.M. Shen, H. Yang, Preparation and characterization of PVDF-SiO<sub>2</sub> composite hollow fiber UF membrane by sol-gel method, *J. Membr. Sci.*, 337 (2009) 257–265.
- [41] J.F. Li, Z.L. Xu, H. Yang, L.Y. Yu, M. Liu., Effect of TiO<sub>2</sub> nanoparticles on the surface morphology and performance of microporous PES membrane, *Appl. Surf. Sci.*, 255 (2009) 4725–4732.
- [42] N.A.A. Hamid, A.F. Ismail, T. Matsuura, A.W. Zularisam, W. J. Lau, E. Yuliwati, M.S. Abdullah, Morphological and separation performance study of polysulfone/titanium dioxide (PSF/TiO<sub>2</sub>) ultrafiltration membranes for humic acid removal, *Desalination*, 273 (2011) 85–92.
- [43] C.S. Feng, B.L. Shi, G.M. Li, Y.L. Wu, Preparation and properties of microporous membrane from poly(vinylidene fluoride-co-tetrafluoroethylene) (F2.4) for membrane distillation, *J. Membr. Sci.*, 237 (2004) 15–24.
- [44] H.D. Wang, R. Xie, C.H. Niu, H. Song, M. Yang, S.A. Liu, L.Y. Chu, Chitosan chiral ligand exchange membranes for sorption resolution of amino acids, *Chem. Eng. Sci.*, 64 (2009) 1462–1473.
- [45] W. Zhao, Y.L. Su, C. Li, Q. Shi, X. Ning, Z.Y. Jiang, Fabrication of antifouling polyethersulfone ultrafiltration membranes using Pluronic F127 as both surface modifier and pore-forming agent, *J. Membr. Sci.*, 318 (2008) 405–412.
- [46] E. Fontananova, J.C. Jansen, A. Cristiano, E. Curcio, E. Drioli, Effect of additives in the casting solution on the formation of PVDF membranes, *Desalination*, 192 (2006) 190–197.
- [47] Y.Y. Nan, W. Jun, Z.Q. Zhu, C.X. Si, Z.H. Xuan, The research of rheology and thermodynamics of organic-inorganic hybrid membrane during the membrane formation, *J. Membr. Sci.*, 311 (2008) 200–207.